

ADDITIONS AND IMPROVEMENTS TO THE RF CAVITY CODE SUPERFISH

S.O. Schriber and R.F. Holsinger*

Atomic Energy of Canada Limited, Research Company
Chalk River Nuclear Laboratories
Chalk River, Ontario, Canada K0J 1J0

Summary

SUPERFISH is a computer code that is used extensively to determine rf properties of rf structures. This paper describes a new post processor for SUPERFISH that determines temperature distributions in the metal enabling high average power rf characteristics for various cooling configurations to be examined. Different materials can be incorporated for different parts of the cavity geometry. Sample results for geometries including drift tube linacs and coupled cavity linacs are presented. Other improvements to the code give electric fields at all vacuum mesh points, normalized RFQ geometry parameters, and transit time factors (T_0 , T_1 , T_2 , S' , \bar{S} , \bar{S}_0 and \bar{S}_0) associated with off-axis electric fields for MAPRO beam dynamics codes.

Introduction

Many design aids are used in the determination of optimum geometrical parameters for rf cavities. The computer code SUPERFISH¹ made a significant impact as a tool for designing cylindrically symmetric cavities when it was first introduced. Since then improvements² have been made to SUPERFISH, such as the treatment of dielectric materials in the rf region, incorporation of a better resonant frequency root finder and the ability to calculate modes and their characteristics in cartesian co-ordinates for non-cylindrically symmetric geometries. The general method was developed further for the code ULTRAFISH³, which calculates properties of azimuthally periodic modes in cylindrically symmetric rf cavities. This paper describes a new post-processor PANT that solves the heat diffusion equation in the metal regions of the rf structure. Some improvements to the SUPERFISH routine FISH for providing parameters of significance to accelerator designers are also described.

The Post-Processor PANT

A requirement usually imposed on rf cavity design is to have rf efficiency as high as possible subject to constraints imposed by rf breakdown, mechanical assembly, beam bore diameter, rf coupling, modes of operation and cooling. Effects of cooling have generally been determined empirically, based on experience and expected system performance. The purpose in developing a new postprocessor for SUPERFISH was to provide the cavity designer with a quantitative analytical tool that could be used to determine cooling characteristics of rf structures, particularly for those operating at high average power. Since SUPERFISH calculates power dissipation on the metal surfaces and uses an irregular triangular mesh it seemed logical to develop a temperature postprocessor that was compatible with SUPERFISH output and the mesh generator. One author (RFH) did most of the development and coding using PANDIRA⁴ as the basic building block - many PANT subroutines are similar to those in POISSON group programs.

The computer code PANT solves the steady state heat diffusion equation for temperatures within the metal allowing for fixed temperature surfaces and symmetry boundary conditions. PANT also determines the associated change in rf efficiency related to temperature induced changes in surface resistivity of the rf

cavity walls. The differential equation (given for a two-dimensional cylindrical r-z geometry) to be solved is

$$\frac{\partial}{\partial r} r \frac{\partial u}{\partial r} + r \frac{\partial^2 u}{\partial z^2} = - \frac{rq}{K}$$

where, K = thermal conductivity in W/(cm·°C) at (r,z)
u = temperature in °C at (r,z)
q = power density in W/cm³ at (r,z).

The main SUPERFISH routines had to be modified to accommodate the requirements of the temperature post-processor. AUTOMESH was modified to define up to five metal regions that are additional to the rf cavity regions. LATTICE was modified to identify all metal region mesh points, particularly those on the metal surface boundary that would be used for both PANT and FISH calculations. Modifications to FISH included the provision for passing rf power at mesh points on the metal walls to PANT where they form the power density terms in the heat equation. TEK PLOT was modified to plot either metal region isotherms or rf cavity fields.

PANT requires input of thermal conductivities for each metal region, boundary symmetry conditions and the temperature in °C for specified boundary surfaces. Constant temperature surfaces are only allowed on the extreme logical boundary. Thermal conductivity for each metal region is allowed to vary spatially as determined from $K = a + bz + cr$ where a, b and c are input coefficients. Alternatively, the condition $K = a$ for $r \leq b$ and $K = c/r$ for $r > b$ may be selected. This latter selection allows the user to represent the effects of radial cooling tubes that penetrate the cavity webs in the radial direction. At present, metal regions forming the rf envelope are assumed to be copper with an electrical resistivity R_T at temperature T given by [$R_T = R_{20} * (1 + 0.00393 * (T-20))$].

A calculation cycle consists of determining mesh point temperatures based on input data and the heat diffusion equations. Once the first cycle temperatures are calculated, the metal boundary source power terms (initially input from FISH) are adjusted to give new wall losses associated with temperature related changes in surface resistivity for each boundary mesh point. If the ratio of new losses to old losses exceeds a user input value (1.05 was used for the cases described below to ensure that maximum temperature increases would be calculated to better than 10% accuracy), the new values are used as source terms and the calculation cycle is repeated. This process continues until the ratio for the last cycle is less than the user specified value. Temperatures and the fractional change in cavity rf loss are output at the end of each cycle.

Since temperatures and associated effects are not needed to the same accuracy as the rf parameters, problem detail and mesh sizes will be dictated by rf requirements (see reference 1). In general, for each calculation cycle PANT requires approximately one-half the computer time that FISH requires for each frequency iteration towards the rf solution.

Code accuracy was verified by comparison with an analytical calculation for a 2294 MHz, 5 cm radius, 3 cm long pillbox cavity with a 3 cm thick cylindrical copper outer wall (outer radius 8 cm). End wall losses

* Field Effects, Inc., PO Box 233, Carlisle, Mass., USA.

were defined to be zero in each case. The temperature difference, ΔT , from the outer radius, r_2 , to the inner radius, r_1 , is given by the analytic solution

$$\Delta T = \ln\left(\frac{r_2}{r_1}\right) * \frac{Q}{L(2\pi K)}$$

where Q is the total power to the metal surface and L is the length of cylinder. With $Q/L = 50$ W/cm the analytic solution yields a ΔT of 0.9590°C for $K = 3.9$ W/(cm $\cdot^\circ\text{C}$). PANT with a coarse 4×10 mesh gave 0.9586°C , in excellent agreement.

Examples of Calculations

Calculations for the following examples used cooling surface temperatures of 30°C , 100% duty factor, thermal conductivities of 3.9 W/(cm $\cdot^\circ\text{C}$) for copper and 0.14 W/(cm $\cdot^\circ\text{C}$) for steel (both assumed to be temperature independent over the range of interest), and the resistivity expression given above. Unless otherwise specified, theoretical rf losses are related to an average on-axis electric field of 1 MV/m.

Results for different geometries are shown to demonstrate the versatility of the code. Twenty equispaced isotherms are shown between the reference outer cooling surface (marked by an arrow) to the highest temperature location (marked by an asterisk).

Figure 1 presents results for a $\beta = 0.65$, 814 MHz shaped cavity under different cooling configurations. The 14.3 cm radius cavity with 0.5 cm half web thickness, 1.9 cm bore radius and 2.3 cm thick outer wall had a 14.8 kW/m power loss along the length of the structure for a zero phase accelerating gradient of 0.8 MeV/m. The figures are to scale so other dimensions can be determined. Peak temperature increases were 19.3°C , 1.6°C , 0.75°C , 1.3°C and 3.3°C for Figs. 1(a) to 1(d) respectively. Figures 1(a) and 1(b) show results for separate circumferential and radial cooling whereas Fig. 1(c) shows the results of the two being combined. Figure 1(d) shows the change in temperature distribution associated with 16 radial cooling tubes (5 mm radius) through the web and 16 longitudinal tubes at the outer surface. Maximum temperature increase to the nose was 0.75°C compared to 1.30°C on the upper cavity radius. Figure 1(e) approximates an end cavity with circumferential cooling and an annular cooling ring located at 5 cm radius. Note that the annular ring could have been placed at a more effective location. Maximum temperature increase to the nose was 2.3°C compared to 3.3°C on the web.

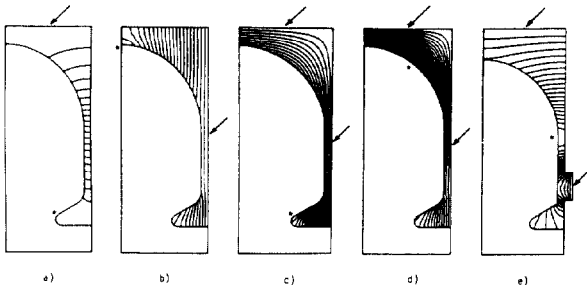


Fig. 1 Isotherms for 814 MHz shaped cavity with a) circumferential cooling, b) radial cooling, c) circumferential and radial cooling, d) sixteen cooling tubes radially and longitudinally and e) circumferential and annular ring cooling. Arrows indicate cooling surfaces and asterisks indicate hottest locations.

In all cases, if the temperature changes related to changes in surface resistivity are ignored, a fractional rf loss multiplier, F , can be determined

$$F = \sqrt{1 + 0.00393 (sE + T - 20)}$$

where T is the outer cooling surface temperature in $^\circ\text{C}$ and sE represents an average structure temperature with E the average on-axis electric field and s a structure proportionality constant in $^\circ\text{C}/(\text{MV}/\text{m})$ based on PANT calculations. The constant s can be used as an indicator of structure cooling suitability - the smaller the constant, the better the cooling. Values of s for configurations of Figs. 1(a) to 1(d) were 5.6 , 0.62 , 0.27 , 0.75 and $1.6^\circ\text{C}/(\text{MV}/\text{m})$, respectively. Clearly radial cooling is very important.

In principle, the fractional change in rf loss can be calculated for any accelerating gradient if s is known. At high powers the simple formula is not exact. For instance, at 8.9 MV/m (167 W/cm 2 radial cooling only as in Fig. 1(b)) the peak calculated outer wall temperature rise of 130°C (with an 11.1% increase in rf loss) becomes 158°C (with a 12.6% increase in rf loss) when resistivity changes are included.

Figure 2 shows isotherms for a 1320 MHz disk-and-washer cavity and a 2450 MHz on-axis coupled cavity. Calculated s parameters for these $\beta = 1.0$ geometries were 0.37 and $3.0^\circ\text{C}/(\text{MV}/\text{m})$ respectively. The 16.6 cm radius disk-and-washer cavity with 0.4 cm half web thickness, 2.7 cm half disk thickness, 2 cm thick outer wall, 1.1 cm bore radius, 14.5 cm disk radius and 8.9 cm radius washer had a 7.5 kW/m power loss for a zero phase accelerating gradient of 0.83 MeV/m. Maximum temperature increase to the washer nose was 1.93°C with 0.29°C to the hottest spot on the disk.

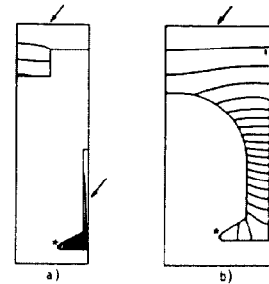


Fig. 2 Isotherms for a) a 1320 MHz disk-and-washer cavity and b) a 2450 MHz on-axis coupled cavity. Arrows indicate cooling surfaces and asterisks indicate hottest locations.

Dimensions for the on-axis coupled cavity of Fig. 2(b) (a 2450 MHz structure for a racetrack microtron) were taken from reference 5. The 4.7 cm outer radius cavity with 0.62 cm thick web, 1.8 cm thick outer wall and 0.7 cm bore radius had a 9.4 kW/m power loss for a zero phase accelerating gradient of 0.855 MeV/m. The temperature increase to the nose without corrections was 7.7°C . For 85% of theoretical rf efficiency and a 1 MeV/m accelerating gradient, the longitudinal dissipation would have been 15.1 kW/m with a corrected temperature increase to the nose of 13°C (12.4°C uncorrected). The factor F is 1.03 for these parameters giving a 3% loss in efficiency. The 13°C temperature increase is in good agreement with another calculation⁶ but is slightly lower than a measured value of 16.5°C . Reasons for this discrepancy are being investigated and may be because the circumference was not flood cooled as assumed in the above calculation.

Figure 3 shows maximum temperature increase at the nose and the rf loss multiplier, F , as a function of power loss in kW/m for the 2450 MHz on-axis coupled cavity. The top of the figure lists the zero phase accelerating gradient for theoretical and 85% of theoretical efficiency. The power density goes beyond what would be considered practical for only circumferential cooling, reaching 116 W/cm 2 . Data with and without

resistivity corrections are shown to illustrate how important this correction becomes at elevated temperatures. The figure also demonstrates that designs to 2.5 MeV/m are possible, even higher if radial cooling was included in the structure. At 2.5 MeV/m, a 93°C temperature increase is predicted to the nose with 94.5 kW/m rf losses. The factor F is 1.085 at this gradient, raising losses to 102.5 kW/m.

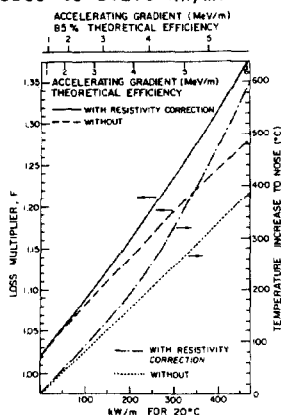


Fig. 3 Loss multiplier and temperature increase as a function of longitudinal power.

Examples of the meshes used in the metal and rf regions for the on-axis coupled cavity and the shaped cavity are shown in Fig. 4.

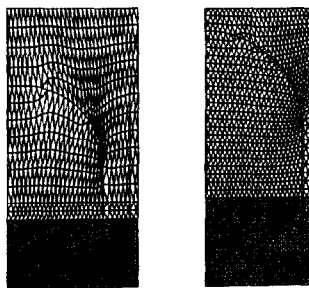


Fig. 4 Meshes for the on-axis coupled cavity and the shaped cavity.

Results of calculations for 200 MHz $\beta = 0.1$ drift-tube linac cavities are shown in Fig. 5. Calculated s parameters for the geometries of Figs. 5(a) to 5(c) were 0.51, 1.7 and 3.1°C/(MV/m). Maximum temperature increases on the 9 cm outer radius drift tube and the 47 cm radius outer wall for the geometry of Fig. 5(a) with a 3 cm thick outer wall and 14 kW/m loss were 1.48°C and 0.23°C respectively. The effects of annular cooling tubes are shown in Fig. 5(b) with maximum temperature increases of 4.0°C and 1.1°C for the drift tube and the outer wall, respectively. Figure 5(c)

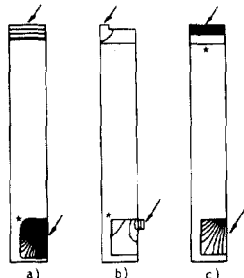


Fig. 5 Isotherms for 200 MHz drift tube cavities with a) outer wall and drift tube cooling, b) tube cooling on the circumference and the drift tube and c) a combination of steel and copper for the outer wall. Arrows indicate cooling surfaces and asterisks indicate hottest locations.

shows the effect of a 2 cm thick copper inner wall attached to 2 cm thick steel wall. Maximum temperature increases for the drift tube and outer wall were 2.0°C and 4.2°C, respectively.

FISH Modifications

FISH has been improved to allow selection of a normalizing factor other than the 1 MV/m average on-axis electric field. Radiofrequency quadrupole (RFQ) geometries have been normalized to a 100 kV potential at the end of the upper vertical vane tip. Output has been expanded to provide stored energy per unit length, rf loss per unit length and voltages on the horizontal and vertical vane tips. Electric field components for all mesh points in the rf region can now be flagged for output, including output of percentage stored energy in the electric fields as a function of mesh row number.

Using the electric fields calculated for mesh points off-axis, the transit time factors⁷ for MAPRO beam dynamics codes (T_0 , T_1 , T_2 , S' , S , \bar{S} , S_0 and \bar{S}_0) were added and can be flagged for output.

Discussion

Improvements to SUPERFISH have made this design tool more versatile. The post-processor PANT calculates temperatures in metal regions and determines changes in rf efficiency of cavities. These two factors are important for the design of high power systems that operate at high duty cycle. The examples described above show that radial cooling is important, resistivity changes lead to increased rf loss and 2.5 MeV/m gradients are possible in 2450 MHz on-axis coupled structures. Future PANT improvements include introduction of materials other than copper as the metal rf interface and a consideration for determining frequency shifts based on temperature changes.

Improvements to FISH routines related to RFQ calculations and MAPRO transit time factors have recently been added to the code. These have proven useful in the comparison of different RFQ geometries, the determination of RFQ dimensional tolerances based on desired quadrant fields and beam dynamics calculations using the MAPRO codes.

References

1. K. Halbach et al., "Properties of the Cylindrical RF Cavity Evaluation Code SUPERFISH", Proc. of 1976 Proton Linac Conf., Atomic Energy of Canada Limited, Report No. AECL-2600, 122 (1976).
2. D.W. Reid et al., "SUPERFISH", Proc. of 1981 Linac Conf., Los Alamos National Laboratory, Report No. LA-9234-C, 99 (1981).
3. R.L. Gluckstern et al., "ULTRAFISH - Generalization of SUPERFISH to $m \geq 1$ ", *ibid.*, 102 (1981).
4. K. Halbach and R.F. Holsinger, "PANDIRA, A Computer Program for the Solution of Anisotropic Field Problems by a Direct Method", to be published.
5. H. Euteneuer, "Design, Performance and Blow-up Properties of the MAMI Structure", Proc. of the Conf. on Future Poss. for Electron Accel., University of Virginia, January 1979, P-1.
6. J. McKeown and J.-P. Labrie, "Heat Transfer, Thermal Stress Analysis and the Dynamic Behaviour of High Power rf Structures", proceedings of this conference.
7. M. Martini and M. Promé, "Computer Studies of Beam Dynamics in a Proton Linear Accelerator with Space Charge", Particle Accelerators 2, 289 (1971).